Materials Advances

ROYAL SOCIETY OF CHEMISTRY

PAPER

View Article Online
View Journal | View Issue

Cite this: *Mater. Adv.*, 2023, 4, 542

Facile preparation of amorphous photonic structure towards rapid temperature sensing and antibacterial textile†

Yun-Liang Ji, Lan-Xing Gao and Yu Tian *

Colloidal photonic crystals (CPCs), a type of chromogenic material, have been widely used in sensing, converting stimuli into discernible color changes. Traditional CPC sensors with ordered structures are subject to angle-dependent structural color, which may lead to the errors in the sensing process. In this study, an amorphous photonic structures (APS) with angle-independent, noniridescent, and highly saturated structural color are successfully fabricated by doping black silver nanoparticles (Ag NPs). The high saturation is attributed to the absorption of incoherent scattered light in the whole visible spectrum uniformly by the added Ag NPs. In addition, based on the APS film, an angle-independent and colorful temperature sensor is developed. Compared with traditional sensors based on photonic crystals, this noniridescent temperature sensor is more accurate and practical because it avoids the color confusion caused by the angle-dependence of the structural color. Furthermore, taking advantage of the spray-coating method, textiles with saturated angle-independent structural colors and antibacterial ability are obtained, extending the application of APS in aseptic packaging and decoration.

Received 15th October 2022,
Accepted 27th November 2022

DOI: 10.1039/d2ma00982j

rsc.li/materials-advances

Introduction

Colloidal photonic crystals (CPCs) are a type of structural chromogenic material formed by periodically stacking materials with different refractive indices in space. In 1987, Yablonovitch and John independently reported creative work on artificial photonic crystals.[1,2] When the wavelength of the incident light matches the photonic band gap (PBG) of the photonic crystal, the incident light will be reflected instead of transmitted, resulting in the generation of structural color when the wavelength is in the visible range.[3,4] Hence, photonic crystals with adjustable lattices are widely used in the display[5,6] and sensing[7] fields. However, the observed structural colors heavily rely on the viewing angles, which may cause sensing errors. In order to solve this problem, spherical CPCs with angle-independent structural colors have been developed and used in the area of sensing. In this field, Weitz and his team developed a spherical photonic crystal hydrogel with temperature sensing ability by immobilizing polystyrene colloids in a hydrogel matrix using microfluidic devices.[8] The spherical colloidal crystal adopted the face-centered-cubic structure, and Bragg reflection was mainly observed at the central sphere of 111 lattice plane, which made the position of the reflection peak independent of the rotation of the sphere, so as to achieve a more accurate temperature sensing effect. However, a more practical and cost-effective way to prepare CPC sensors with greater accuracy was still needed. Inspired by nature, the colorful and brilliant structural colors in the biological world, such as the feathers of plum-throated cotinga[9] and macaws[10] and the skin of turkeys,[11] have attracted extensive research attention. These beautiful colors come from the amorphous arrangement of keratin or skin cells. In contrast to ordinary CPCs, such amorphous photonic crystals are characterized by the short-range order of the construction units arranged on a scale comparable to the wavelength of visible light. Compared with the iridescence of photonic crystals, the structural color of amorphous photonic structures (APS) has noniridescent characteristics with angle-independence.[12] Therefore, a sensor based on APS can easily achieve accurate sensing. However, the structural color of APS depends on the short-range ordering and coherent scattering effect of nanoparticles, for which the coherent scattering effect is much weaker than Bragg diffraction, and even weaker than incoherent scattering, leading to a macroscopic white appearance.[13–15] Therefore, it is still a challenge to prepare APS with vivid noniridescent structural color. An inspiring phenomenon in nature is the existence of melanin in the feathers of *Meleagris gallopavo*, making them appear bright yellow.[16] Therefore, to prepare APS films with bright structural colors it is key not only to avoid the orderly assembly of colloidal

Department of Chemistry, Key Laboratory of Surface & Interface Science of Polymer Materials of Zhejiang Province, Zhejiang Sci-Tech University, Hangzhou 310018, China. E-mail: tianyu_zstu@zstu.edu.cn

† Electronic supplementary information (ESI) available. See DOI: https://doi.org/10.1039/d2ma00982j

crystals, but also to add appropriate black dopant to absorb incoherent scattered light and improve the saturation of the structural color. Common black dopants, including carbon black,[17] cuttlefish ink,[18] graphene,[19] polydopamine,[20] acetylene black,[21] *etc.* have been widely researched. However, appropriate methods to prepare APS films and extend their applications are still in high demand.

Here, we chose silver nanoparticles (Ag NPs),[22] a type of metal nanoparticle with good thermal conductivity[23] and antibacterial effects,[24] as the black dopant, and poly(styrene-butyl acrylate-methacrylic acid) (P(St-BA-MAA)) colloidal particles with a shell–core structure as the building units to prepare an APS temperature sensor and APS textiles. In this field, Lai *et al.*[25] prepared photonic crystal colored films with a high concentration of Ag NPs by a self-assembly process using the gravity sedimentation method. A high concentration of Ag NPs are deposited at the bottom of the substrate and act as black materials to absorb background light and scattered light. We first combined Ag NPs with APS film through straightforward spray-coating and hand-writing methods to identify the ability of Ag NPs to promote the saturation of APS film color (Scheme 1(a) and (b)). A multi structural color pattern can be easily realized on common substrates,[26] such as glass sheet and polyethylene terephthalate (PET) substrates. In addition, we developed a temperature sensor by introducing the poly(*N*-isopropylacrylamide) (PNIPAm) hydrogel into the APS film with the Ag NPs (Scheme 1(c)). The Ag NPs can promote heat conduction in the PNIPAm hydrogel film, which provides a foundation for the rapid temperature sensing effect. The temperature sensor displayed vivid structural color and noniridescent color. The change of ambient temperature can be quickly identified through the variable color of the APS hydrogel sensor, which avoids the confusion of color change caused by angle-dependence in traditional photonic crystal sensors. In addition, we used the spray-coating method to load APS/Ag on the surface of the fibers of the flexible textile. Because of the excellent antibacterial effect of the silver nanoparticles, the APS/Ag textiles we prepared had significant antibacterial properties (Scheme 1(d)).

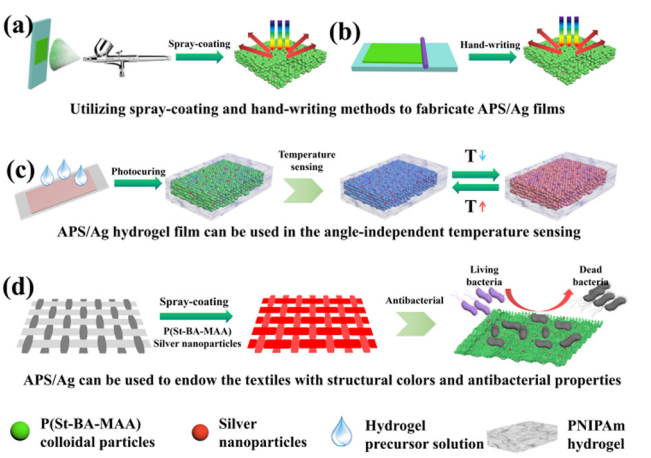

Scheme 1 Facile fabrication of APS films with noniridescent structural colors by doping Ag NPs utilizing the methods of (a) spray-coating and (b) hand-writing. (c) Schematic illustration of the preparation of the Ag NP-doped temperature sensor produced by embedding the colloidal particles in the NIPAm hydrogel. (d) Antibacterial textiles constructed by the spray-coating method.

Experimental

Chemicals and materials

Styrene (St) was provided by Aladdin and was purified by distillation under reduced vacuum to remove the inhibitor before use. Polyvinyl pyrrolidone (PVP) was provided by Aladdin. Potassium persulfate (KPS), α-methacrylic acid (MAA), butyl acrylate (BA), potassium persulfate, sodium dodecyl sulfate (SDS) *N*-isopropylacrylamide (NIPAm), sodium dodecylbenzene sulfonate (SDBS), *N*,*N*′-methylenebisacrylamide (MBA) and 2-hydroxy-4′-(2-hydroxyethoxy)-2-methylpropiophenone (2959) were provided by Macklin. Silver nanoparticles with a size of around 79.6 nm were provided by Shanghai Xiangtian Nano Materials Co., Ltd, China. All chemical reagents used were analytical reagents.

Preparation of poly(styrene-butyl acrylate-methacrylic acid) colloidal particles

P(St-BA-MAA) colloidal particles with sizes of 292.7 nm, 285.5 nm, 271.6 nm, 266.6 nm, 258.5 nm, and 230.3 nm with PDI less than 0.05 were prepared by emulsion polymerization (Fig. S1a–f and Table S1, ESI†). A typical procedure for the preparation of P(St-BA-MAA) colloidal particles with a diameter of 230.3 nm is as follows: 0.25 g of PVP and 5 g of St were dissolved in 135 mL of deionized (DI) water, and then the mixture was added to a four-necked round-bottomed flask. The flask was then put into an oil bath and heated to 98 °C under gentle stirring. 0.04 g of KPS dissolved in 15 mL of DI water was added to the flask at a rate of 1 mL min^{-1} to initiate the polymerization. After 1.5 h, 0.5 g of BA and 0.5 g of MAA were added to the flask dropwise. The reaction was terminated after about 2.5 h. The resulting latex was purified by filtration with a nylon net and further purified and concentrated by centrifugation at 12 000 rpm with DI water three times.

Preparation of APS films by spray-coating

10 wt% P(St-BA-MAA) colloidal particles with diameters of 258.5 nm (main particles), 1 wt% P(St-BA-MAA) colloidal particles with diameters of 230.3 nm, 1 wt% Ag NPs and 1 wt% SDBS were dispersed in water and treated by sonication for at least 1 hour. Then the mixture was sprayed onto glass substrates with an airbrush equipped with a 0.5 mm outlet nozzle. The purpose of mixing P(St-BA-MAA) particles with two sizes is to suppress the ordered arrangement of particles and to obtain short-range ordered APS, to help reduce angle-dependence.[27] The film appearing on the substrate showed an obvious green structural color after the water had evaporated. The procedures to prepare red and blue colored APS films were similar to the above, except 292.7 nm (main particles) and 258.5 nm P(St-BA-MAA) colloidal particles were used for the red APS film, and

230.3 nm (main particles) and 266.6 nm P(St-BA-MAA) colloidal particles were used for blue APS film.

Preparation of APS films by the hand-writing method

First, 40 wt% 258.5 nm P(St-BA-MAA) colloidal particles (main particles), 4 wt% 230.3 nm P(St-BA-MAA) colloidal particles, 4 wt% Ag NPs and 4 wt% SDBS were mixed and treated with ultrasound for 2 hours, then stirred for 5 minutes. The mixture was then coated on the surface of a transparent PET film with a 10 μm-depth roll bar. A bright green structural colored film was obtained after drying in an oven at 65 °C for 1 minute. With the other conditions remaining unchanged, 40 wt% 292.7 nm (main particles) and 4 wt% 258.5 nm P(St-BA-MAA) colloidal particles were used to obtain a red structural colored film. 40 wt% 230.3 nm (main particles) and 4 wt% 266.6 nm P(St-BA-MAA) colloidal particles were used to obtain a blue structural colored film.

Construction of APS temperature sensor with noniridescent structural color

For the preparation of a temperature sensor, 40 wt% 230.3 nm colloidal particles (main particles), 5 wt% 266.6 nm colloidal particles, 0.125 wt% Ag NPs, 0.125 wt% SDBS, 10% NIPAm, 1 wt% MBA and 1 wt% photoinitiator 2959 were mixed and sonicated for 2 hours and then stirred for 5 minutes. The obtained mixture was transferred to a gap between two glass slides with an interval of 0.3 mm, and cured under 365 nm ultraviolet light for 5 minutes to obtain an APS hydrogel composite temperature sensor. For the construction of patterned hydrogels, square, round and triangular gaps in the mask were filled with the above mixture of hydrogel precursors and then cured with UV light for 5 minutes.

Preparation of antibacterial textile with bright structural color

For the preparation of APS/Ag textiles, 10 wt% 230.3 nm colloidal particles (main particles), 1 wt% 266.6 nm colloidal particles, 1 wt% Ag NPs and 1 wt% SDBS were sonicated for 2.5 hours and then stirred for 5 minutes. The mixture was loaded on the surface of brushed polyester cotton by the spray-coating method, and then dried at 80 °C for five minutes to obtain APS/Ag textiles with bright structural color.

Test of antibacterial effect

Consistent with the previously reported literature,[28] the surface antibacterial activities of the original textiles (negative control), textiles coated with APS film but without Ag NPs (APS textiles) and textiles coated with APS film doped with Ag NPs (APS/Ag textiles) against representative bacteria, namely *Escherichia coli* (*E. coli*) and *Staphylococcus aureus* (*S. aureus*) were tested. In a typical procedure, a textile sample was put into a sterile test tube. 50 μL of bacterial suspension with a concentration of 10^6 CFU mL^{-1} was dropped onto the surface of the textile and the culture was put in an incubator at 37 °C for 2 hours. Then, the bacteria were rinsed by 950 μL of sterilized culture medium. Then, 200 μL of the bacterial suspension of the sample was inoculated onto an agar plate and incubated at 37 °C for 18 h. The experiment was repeated three times for each group and the colony forming units (CFU) were counted and used to evaluate the antibacterial ability of the textiles using the following equation:

$$\log \text{reduction} = \log(\text{cell count of negative control}) - \log(\text{survivor count of samples})$$

Characterization

The reflection spectra of the photonic crystal films at varying angles were recorded by an optical microscope equipped with a fiber optic spectrometer (Ocean Optics, USB4000). The microstructures of the P(St-BA-MAA) colloidal particles, APS films, hydrogel and textiles were characterized using a scanning electron microscope (SEM) (Hitachi S-4800). Particle size distribution and PDI measurements were conducted using a Deisa Nano instrument. Photographs were taken using an optical microscope (SZMN, 48 MP Full HD Camera). X-ray diffraction (XRD) was conducted on a Bruker AXS D8 Discover. UV-vis absorbance tests were carried out using a VARIAN ECHNOLOGIES Cary 50 and SHIMADZU UV-2700.

Results and discussion

Preparation and optical properties of noniridescent APS films

To investigate how the size of the Ag NPs influences the saturation, APS films doped with Ag NPs with diameters of 19.3 nm, 49.1 nm, and 79.6 nm were prepared. It can be seen from the particle size distribution diagram (Fig. S2, ESI†) that these three Ag NPs have relatively uniform particle sizes. From the UV-vis absorbance spectra of the Ag NPs powders with different sizes and their mixtures with P(St-BA-MAA) emulsion (Fig. S3, ESI†), it can be seen that absorption in the range of 400 nm to 700 nm can be achieved for all the above samples, which enables the prepared APS/Ag films to absorb incoherently scattered light, so that the films have higher structural color saturation (Fig. S4, ESI†). However, the high absorbance will inevitably compromise the brightness of the structural color. Thus the 79.6 nm Ag NPs with relatively weak absorbance were selected as the black dopant to balance the saturation and the brightness.

Monodisperse P(St-BA-MAA) colloidal particles have soft shells and negative charges, which means they have high monodispersity and can be stably dispersed in water, which is conducive to the formation of obvious structural color.[29] Moreover, submicrospheres with soft polymer shells are easy to adhere to yarn, fibers and their adjacent sub-microspheres to improve the bonding strength between amorphous photonic crystals and textiles.[30] P(St-BA-MAA) colloidal particles with different particle sizes were fully mixed with 79.6 nm Ag NPs by ultrasound and stirring and then sprayed evenly onto the cover glass by the spray-coating method. Due to the negative charges on the surfaces,[31] the Ag NPs cannot be completely dispersed in the P(St-BA-MAA) colloidal emulsion. Thus, SDBS was added to improve the dispersibility of the Ag NPs to form a uniform APS precursor (Fig. S5, ESI†). The rapid evaporation of water and the addition of particles of different sizes inhibited the self-assembly of the colloidal particles into an ordered structure, which resulted in

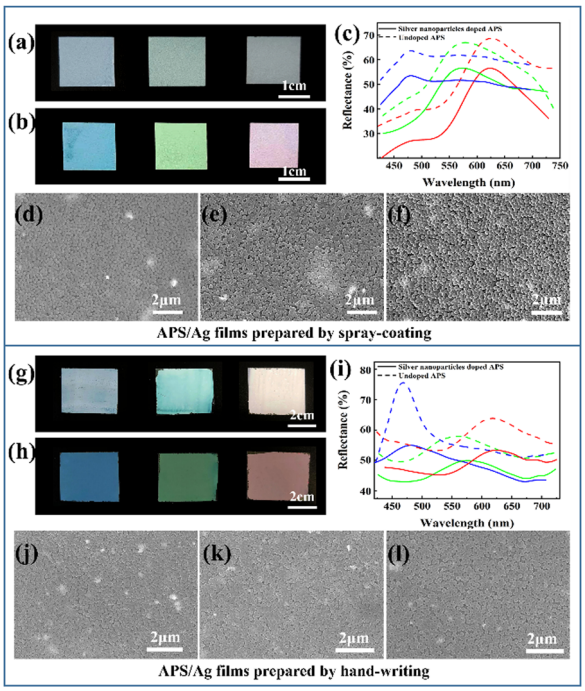

Fig. 1 Optical images of APS films without Ag NPs (a) and with Ag NPs (b) prepared by spray-coating. (c) Reflection spectra of APS films doped with and without Ag NPs. SEM images of (d) blue, (e) green and (f) red structural colored films doped with Ag NPs. Optical images of APS films without (g) and with (h) Ag NPs prepared by hand-writing. (i) Reflection spectra of structural colored films doped with and without Ag NPs. SEM images of (j) blue, (k) green and (l) red structural colored films doped with Ag NPs.

short-range order of the distribution of the colloidal particles. Comparing Fig. 1(a) and (b), it can be seen that the saturation of the APS films with Ag NPs are much higher than that of the APS film without Ag NPs. This means that the doped Ag NPs are able to absorb the strong incoherently scattered light in the APS films and enhance the structural color saturation effectively. We also investigated the influence of the amount of added Ag NPs on the structural color of the APS film. Compared with 0.5 wt%, 0.8 wt% and 1.2 wt%, the film doped with 1 wt% Ag NPs showed more vivid structural color (Fig. S6, ESI†). By controlling the particle size of the main P(St-BA-MAA) colloidal particles in the range of 230.3 nm to 292.7 nm, adjustable structural colors can be obtained in the visible spectrum range. Fig. 1(c) shows reflection spectra of the obtained blue, green and red APS films doped with and without Ag NPs. It can be seen that APS films without Ag NPs have stronger reflection intensities than those with Ag NPs, which is due to the fact that Ag NPs can absorb incoherently scattered light as well as partially coherently scattered light, leading to a decrease in the intensity of the reflected light. The SEM images of the Ag NP-doped blue, green and red colored APS films are shown in Fig. 1(d)–(f), in which can be seen that the colloidal particles in the three films are all in a short-range ordered arrangement.

Another method, namely hand-writing, was utilized to fabricate APS films with different structural colors on the PET substrate. Similar to above, two types of monodispersed colloidal particles of P(St-BA-MAA) with different particle sizes were fully mixed with 79.6 nm Ag NPs by ultrasound and stirring. Then, the mixed emulsion was evenly scratched onto the surface of the PET film with a roll bar, and then dried in an oven at 65 °C for 1 minute to obtain APS films. The formulation of a typical green structural colored film prepared by the hand-writing method is 40 wt% 258.5 nm P(St-BA-MAA) colloidal particles (main particles), 4 wt% 230.3 nm [P(St-BA-MAA)] colloidal particles, 4 wt% Ag NPs with a particle size of 79.6 nm and 4 wt% SDBS. The high solid content of the emulsion endowed the mixture with high viscosity and rapid assembly at 65 °C, which effectively inhibits the self-assembly of the colloidal particles into ordered structures. Similar results show that the APS film doped with Ag NPs shows a clearer vivid structural color and lower reflected intensity than those of the APS film without Ag NPs (Fig. 1(g)–(i)). Compared with the film obtained by spray-coating, this film has a brighter structural color and higher reflectivity, which can reach a maximum of 77% for the blue film (Fig. 1(h) and (i)). The short-range ordered arrangement of the obtained films prepared by the hand-writing method can also be observed in the SEM images in Fig. 1(j)–(l). SEM-EDS mapping of the Ag NP-doped APS films suggests that the Ag NPs are partly agglomerated and well dispersed in the P(St-BA-MAA) matrix (Fig. S7 and S8, ESI†). Due to the small thicknesses of the films constructed by spray-coating, the reflectivities of the APS films are low. However, blue films constructed by the hand-writing method have higher reflectivity and narrower reflection peaks. In this regard, we investigated the reflection spectra of photonic crystals with ordered structures constructed using P(St-BA-MAA) colloidal particles of one size. Similar results showing that the blue film has higher reflectivity and narrower reflection peaks were also observed (Fig. S9, ESI†). The high reflection intensity of the blue films may be because the small size of the building blocks generates more layers in the photonic structure, while with the same concentration in the construction of green and red films, the particles are larger. The blue films have a narrower FWHM, probably because the lower PDI (0.026) of the P(St-BA-MAA) colloidal particles for the preparation of the blue film than those for that of the green and red films (0.047 and 0.045) may cause the scattering of light with a smaller range of wavelengths. In the XRD results (Fig. S10, ESI†), no clear silver oxide signals were observed, suggesting that the Ag NPs played a decisive role in improving the structural color saturation of the APS film.

Optical properties of noniridescent structural colored films with multiple patterns

Blue, green and red structural colored films constructed on the surface of PET film by hand-writing show noniridescent and angle-independent structural color. Under natural light, the appearance of the structural color remains almost unchanged at detection angles of 60°, 45°, 30° and 15° (Fig. 2(a)). The angle-independent structural color of the film is also shown in the reflection spectra of the typical green film (Fig. 2(b)). The non-iridescent structural color comes from the incoherent scattering of light at a specific wavelength, which is due to the short-range order of the APS.[17,32] Since there is no preferred direction in the APS, the coherently scattered light is isotropic in all directions.

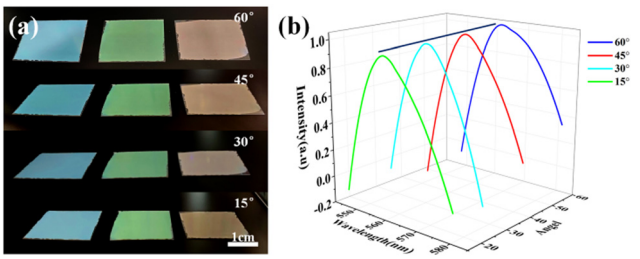

Fig. 2 Angle-independent structural color of the APS/Ag film. (a) Photos of three structural colored films produced by the hand-writing method at viewing angles of 60°, 45°, 30° and 15° (b) Reflection spectra of the green film at viewing angles of 60°, 45°, 30° and 15°. The viewing angles refer to the angles between the reflected light and the horizontal plane.

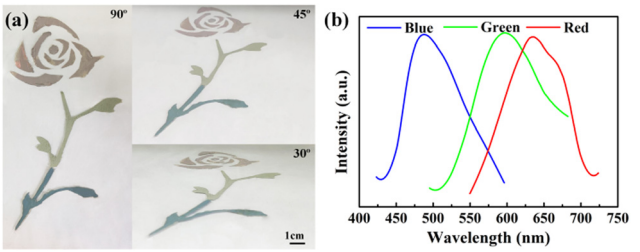

Fig. 3 A colorful structural color pattern constructed on PET film by the hand-writing method. (a) The pattern of a 'rose' at viewing angles of 60°, 45° and 30°. (b) Reflection spectra of three colors. The viewing angles refer to the angles between the reflected light and the horizontal plane.

Under natural light, the angle-dependence of the color appearance is eliminated. Patterns with bright structural colors can be easily constructed by the hand-writing method. Fig. 3(a) shows 'rose' patterns with blue, green and red structural colors on the PET film. The pattern shows the characteristics of angle-independence. Meanwhile, the APS pattern on PET, a type of flexible substrate, demonstrates the practical application of this type of structural color in decorative coatings and functional optical devices.[33–35]

Temperature sensor with angle-independent PBG

In contrast to traditional iridescent photonic crystal sensors, the bright noniridescent structural colors generated by the APS films can be used for accurate and convenient sensing on account of their angle-independent PBG.[36,37] Fig. 4(a) shows a schematic diagram of the temperature sensing of the composite hydrogel film constructed by using 40 wt% P(St-BA-MAA) colloidal particles with diameters of 230.3 nm as the main particles in the PNIPAm hydrogel. The hydrogen bonds generated among the hydrophilic amide groups are greatly affected by temperature, which could affect the hydrophilicity of the hydrogel and lead to a phase transition.[38–40] The lattice of the P(St-BA-MAA) particles in the hydrogel will change with the phase transition, resulting in the structural color changing, in order to realize the response to the temperature. In Fig. 4(b), when the ambient temperature changed form 24 °C to 38 °C, the color of the APS hydrogel film changed from red to bluish green and returned to the red structural color when the environment temperature decreased to 24 °C. In such a process, the Ag NPs acted as a key heat conduction node, which gave the sensor a fast sensing effect. Cyclic temperature sensing was performed to demonstrate the reversibility and stability of the hydrogel temperature sensor. The six cycles at 24 °C and 38 °C repeatedly showed that the hydrogel temperature sensor is durable, and the fastest response time was about 11 seconds (Fig. S11, ESI†). A slight fluctuation in the reflection spectra could be attributed to the stability of the environment and the structure changing inside the hydrogel sensor after each cycle. Fig. 4(c) and (d) show the change in the reflection peak of the APS/Ag hydrogel film in the temperature sensing process. It can be seen that the reflection peak blue-shifts from 602 nm to 555 nm when the temperature is changed from 24 °C to 42 °C, and red-shifts to 602 nm when the temperature is decreased from 42 °C to 24 °C. The reversible color and corresponding reflection peak changes indicate the reusability of our obtained APS/Ag temperature sensor. The SEM image shows that the APS/Ag hydrogel possesses a short-range ordered arrangement of the building units (Fig. 4(e)), and in the inserted SEM image in Fig. 4, we can see that the random particles are all covered by the hydrogel networks, making a vital contribution to the fast structural color change in the temperature sensing. Significantly, this APS/Ag hydrogel temperature sensor retained angle-independent characteristics in the sensing process (Fig. S12, ESI†).

Masks were applied to construct patterned hydrogels with temperature sensing effects (Fig. 4(f)–(h)). When the temperature of the patterned hydrogel in water changed from 24 °C to 38 °C, its color changed from red to green, and a slight deformation of the patterned hydrogel due to water loss was noted. This type of noniridescent temperature sensor based on amorphous photonic crystals with bright structural color can provide an accurate and convenient sensing platform for chemical, physical and biological stimuli.[41–43]

APS/Ag antibacterial textiles

The soft polymer shells of the P(St-BA-MAA) nanoparticles enable them and the Ag NPs to adhere firmly to the textile fibers. We loaded P(St-BA-MAA) and Ag NPs on the textile fibers by the spray-coating method, and obtained angle-independent structural colored textiles (Fig. 5(a) and (b)). Due to the doping of the Ag NPs, the saturation of the structural color of the APS/Ag textiles is much higher than that of the APS textiles without Ag NPs (Fig. S13, ESI†). From the SEM images in Fig. 5(c)–(e), it can be seen that the colloidal particles were assembled on the surface of the fabrics and partly inside the yarns in a short-range ordered arrangement. After folding, turning and crimping, there is no partial loss or change in the structural color (Fig. 5(f)), which indicates that the P(St-BA-MAA) particles and silver nanoparticles are firmly attached to the fiber, which is conducive to the stability of the structural color of the APS/Ag textile.[44,45] Interestingly, the APS/Ag textiles have excellent antibacterial effects. After bacteria (*S. aureus* and *E. coli*) come into contact with the Ag NPs on the APS/Ag textiles, the shells of the bacteria will become unstable or damaged, leading to leakage of the cellular content, and the subsequent death of

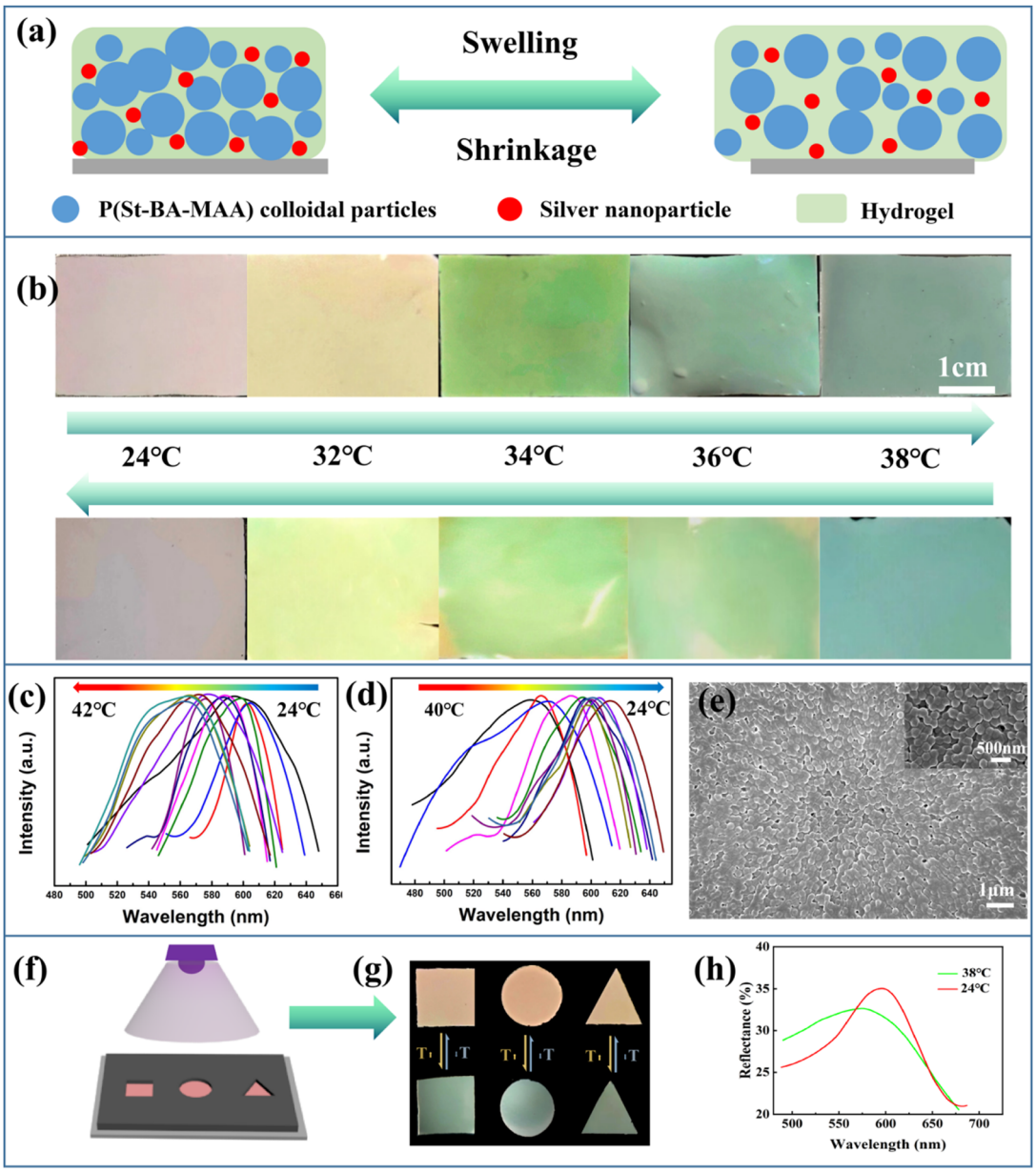

Fig. 4 Performance of the APS/Ag hydrogel film composite temperature sensor doped with Ag NPs. (a) Schematic diagram of hydrogel sensing. (b) Photos of brilliant structural color sensors that change reversibly when the temperature changes. (c) and (d) Reflectance spectra of the temperature sensor with reversible temperature changes. (e) SEM image of the APS/Ag hydrogel composite sensor doped with Ag NPs. (f) Masks were applied to construct patterned hydrogels with temperature sensing effects. (g) Photos of square, round and triangular hydrogels at 24 °C (top) and 38 °C (bottom). (h) Reflection spectra showing the color change process of the square patterned hydrogel.

the bacteria (Fig. 5(g)).[46,47] It can be seen from the results of the antibacterial tests in Fig. 5(h) and (i) that the APS textiles without Ag NPs have an antibacterial effect in comparison with the negative control. A possible reason for this is that the slightly acidic environment caused by the carboxyl groups on the surfaces of the P(St-BA-MAA) particles makes the survival of bacteria unfavorable.[48,49] However, the APS/Ag textiles can kill almost all of the bacteria, showing excellent antibacterial activity. A qualitative evaluation of the antibacterial activity is made by calculating the logarithmic reduction value of the bacteria. From Fig. 5(j) and (k) it can be seen that for the APS/Ag textiles, the logarithmic reduction values for *S. aureus* and *E. coli* reached 2.55 and 2.16, respectively, meaning that more than 99% of the bacteria were killed, demonstrating excellent antibacterial effects.

Conclusions

In this work, we reported the fabrication of an APS film with bright noniridescent structural color, which allowed the absorbance of incoherently scattered light and partially coherently

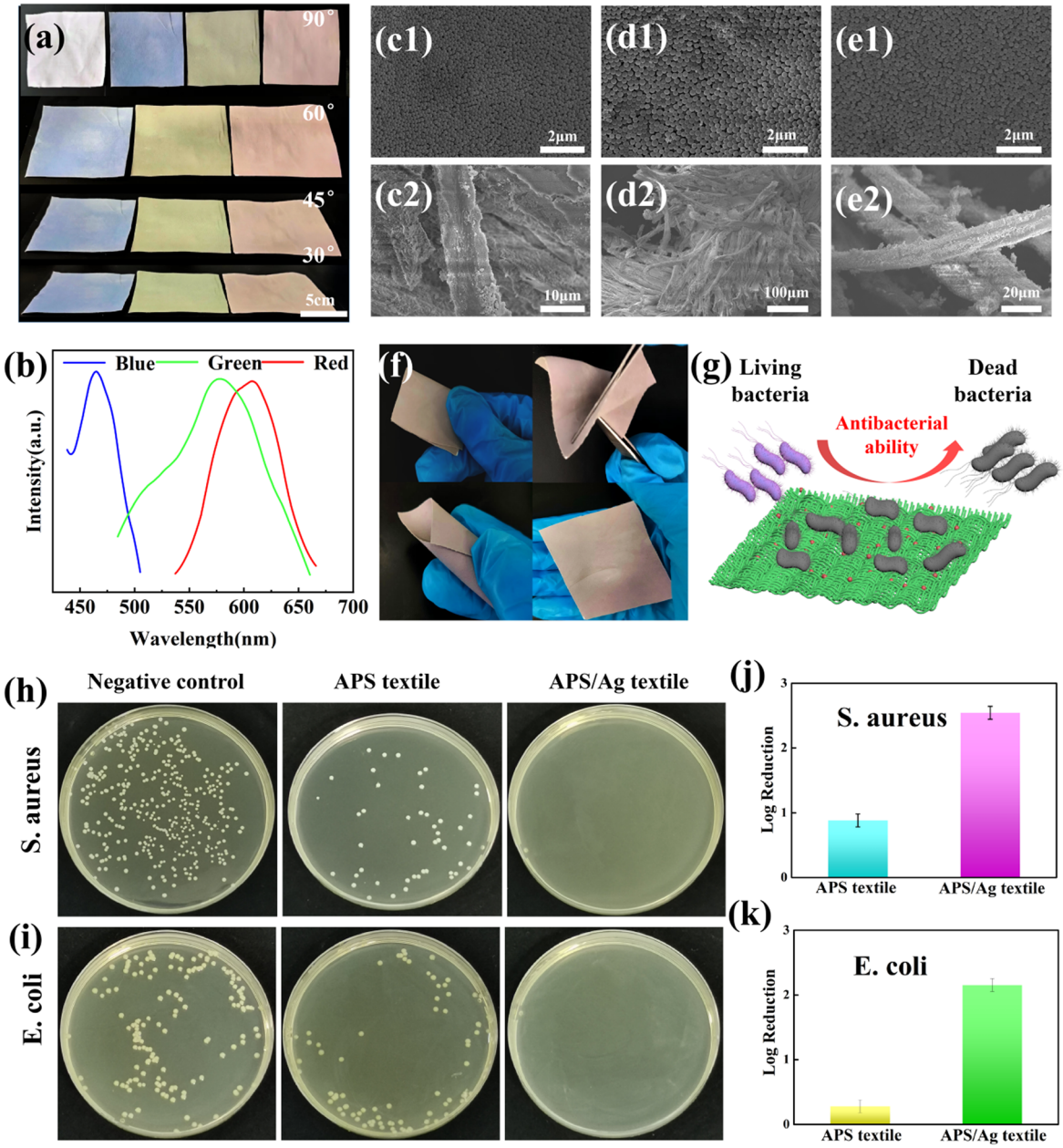

Fig. 5 Preparation of APS/Ag textiles. (a) Photos of APS/Ag textiles with blue, green and red structural colors at viewing angles of 90°, 60°, 45° and 30°. (b) Reflectance spectra of APS/Ag textiles with three structural colors of blue, green and red. SEM image of blue (c1), (c2), green (d1), (d2) and red (e1), (e2) structural colored APS/Ag textiles. (f) Pictures showing folding, turning, crimping and restoring of the APS/Ag textiles. (g) Schematic illustration showing the antibacterial effect of the APS/Ag textiles. (h and i) Comparative photos showing the antibacterial effect of the textile, APS textile and APS/Ag textile against *S. aureus* and *E. coli*. Antibacterial ability against *S. aureus* (j) and *E. coli* (k). The viewing angles refer to the angles between the reflected light and the horizontal plane.

scattered light by Ag NPs in a photonic crystal system. The uniform light absorption characteristics of the Ag NPs particles play an important role in improving the brightness and saturation of the structural color. Using simple spray-coating and hand-writing methods, colorful APS/Ag films with bright structural colors can be constructed on glass or flexible PET film, which favors the application of APS films in decoration, packaging, coatings, pigments, displays and other color related fields. Furthermore, we constructed an APS/Ag hydrogel temperature sensor by incorporating building blocks into a PNIPAm hydrogel. The sensor could indicate a change of temperature through adjustable structural color rapidly (within 11 s), thanks to the good heat conduction of the Ag NPs. Compared with the traditional photonic crystal sensing platform based on long-range ordered structure and iridescent color, this temperature sensor with bright noniridescent structural color is more efficient, more accurate and more practical, because it can avoid the confusion caused by the angle-dependence of structural color.

Furthermore, due to the antibacterial effect of Ag NPs, the textiles have bright structural colors and excellent antibacterial properties, which may expand the application of APS films in the fields of aseptic packaging and decoration.

Author contributions

Yun-Liang Ji: conceptualization, investigation, methodology, writing original draft. Lan-Xing Gao: investigation. Yu Tian: writing-review and editing, conceptualization, funding acquisition, supervision. All the authors were involved in the discussion of the results, and have read and approved the final manuscript.

Conflicts of interest

There are no conflicts to declare.

Acknowledgements

This research was supported by Zhejiang Provincial Natural Science Foundation of China under Grant No. LQ22B060001 and Zhejiang Sci-Tech University (21062256-Y).

Notes and references

1 S. John, *Phys. Rev. Lett.*, 1987, **58**, 2486–2489.
2 E. Yablonovitch, *Phys. Rev. Lett.*, 1987, **58**, 2059–2062.
3 Z. Cai, Z. Li, S. Ravaine, M. He, Y. L. Song, Y. Yin, H. Zheng, J. Teng and A. Zhang, *Chem. Soc. Rev.*, 2021, **50**, 5898–5951.
4 S. M. Liu, Y. Yang, L. B. Zhang, J. P. Xu and J. T. Zhu, *J. Mater. Chem. C*, 2020, **8**, 16633–16647.
5 Y. H. Li, Z. W. Liu, K. Zhu, L. Q. Ai, P. Jia, N. Wu, H. T. Yu, J. Q. Wang, X. Yao, J. M. Zhou and Y. L. Song, *Adv. Mater. Interfaces*, 2021, **8**, 2101281.
6 Y. H. Li, Y. X. Mao, J. H. Wang, Z. W. Liu, P. Jia, N. Wu, H. T. Yu, J. Q. Wang and Y. L. Song, *Nanoscale*, 2022, **14**, 8833–8841.
7 J. M. Zhou, P. Han, M. J. Liu, H. Y. Zhou, Y. X. Zhang, J. K. Peng, Y. Wei, Y. S. Song and X. Yao, *Angew. Chem., Int. Ed.*, 2017, **56**, 10462–10466.
8 T. Kanai, D. Lee, H. C. Shum and D. A. Weitz, *Small*, 2010, **6**, 807–810.
9 R. O. Prum, R. H. Torres, S. Williamson and J. Dyck, *Nature*, 1998, **396**, 28–29.
10 H. Yin, B. Dong, X. Liu, T. Zhan, L. Shi, J. Zi and E. Yablonovitch, *Proc. Natl. Acad. Sci. U. S. A.*, 2012, **109**, 12260.
11 R. O. Prum and R. H. Torres, *J. Exp. Biol.*, 2003, **206**, 2409–2429.
12 Y. Zhang, P. Han, H. Zhou, N. Wu, Y. Wei, X. Yao, J. Zhou and Y. L. Song, *Adv. Funct. Mater.*, 2018, **28**, 180258.
13 S. Gottardo, R. Sapienza, P. García, A. Blanco, D. S. Wiersma and C. López, *Nat. Photonics*, 2008, **2**, 429–432.
14 P. D. García, R. Sapienza, A. Blanco and C. López, *Adv. Mater.*, 2007, **19**, 2597–2602.
15 E. S. Goerlitzer, R. N. K. Taylor and N. Vogel, *Adv. Mater.*, 2018, **30**, 1706654.
16 C. M. Eliason and M. D. Shawkey, *J. R. Soc., Interface*, 2012, **9**, 2279.
17 Y. Takeoka, S. Yoshioka, A. Takano, S. Arai, K. Nueangnoraj, H. Nishihara, M. Teshima, Y. Ohtsuka and T. Seki, *Angew. Chem., Int. Ed.*, 2013, **52**, 7261–7265.
18 Q. H. Xu, H. Wang, F. F. Fu, C. H. Liu, Z. Y. Chen and Y. J. Zhao, *J. Nanosci. Nanotechnol.*, 2018, **18**, 4834–4840.
19 J. L. Yu, C. H. Lee and C. W. Kan, *Nanomaterials*, 2021, **11**, 949.
20 X. W. Zhu, T. C. Wei, M. S. Mia, T. L. Xing and G. Q. Chen, *Colloids Surf., A*, 2021, **622**, 126651.
21 F. Wang, F. Q. Guo, Y. Xue, H. J. Luo and J. F. Zhu, *J. Coat. Technol. Res.*, 2021, **18**, 489–499.
22 Y. L. Li, W. Y. Duan, X. G. Lu, S. Yang and X. X. Wen, *Opt. Mater.*, 2019, **94**, 423–429.
23 S. K. Wang, D. Haldane, P. Gallagher, T. Liu, R. Liang and J. H. Koo, *Composites, Part B*, 2014, **61**, 172–180.
24 S. Balasubramanian, U. Jeyapaul and S. M. J. Kala, *Int. J. Nanosci.*, 2019, **18**, 1850011.
25 C. F. Lai and Y. C. Wang, *Crystals*, 2016, **6**, 61.
26 C. Wang, X. Lin, C. C. Schafer, S. Hirseman and J. P. Ge, *Adv. Funct. Mater.*, 2020, **31**, 2008601.
27 A. Kawamura, M. Kohri, S. Yoshioka, T. Taniguchi and K. Kishikawa, *Langmuir*, 2017, **33**, 3824–3830.
28 L. Bai, Y. Jin, X. Shang, H. Jin, Y. Zhou and L. Shi, *J. Mater. Chem. A*, 2021, **9**, 23916–23928.
29 L. Chai, S. Hong, S. Sun, H. Li, G. Liu, J. Z. Shao and L. Zhou, *Dyes Pigm.*, 2021, **193**, 105928.
30 G. Liu, L. Zhou, G. Zhang, L. Chai, Y. Li, Q. Fan and J. Z. Shao, *J. Mater. Sci.*, 2016, **51**, 8953–8964.
31 A. N. Vasiliev, E. A. Gulliver, J. G. Khinast and R. E. Riman, *Surf. Coat. Technol.*, 2009, **203**, 2841–2844.
32 S. F. Liew, J. Forster, H. Noh, C. F. Schreck and H. Cao, *Opt. Express*, 2011, **19**, 8208.
33 Z. Y. Wang, C. D. Wang, H. B. Hou, W. S. Liu, R. Nian, H. G. Sun, X. Chen and G. L. Cui, *Appl. Surf. Sci.*, 2019, **479**, 1014–1020.
34 Y. G. Kim, S. Park, Y. H. Choi, S. H. Han and S. H. Kim, *ACS Nano*, 2021, **15**, 12438–12448.
35 C. Liu, A. Q. Xie, G. X. Li, Q. Li, C. F. Wang, L. Zhu and S. Chen, *ACS Appl. Polym. Mater.*, 2021, **3**, 6130–6137.
36 X. Y. He, Y. N. Gu, B. R. Yu, Z. W. Liu, K. Zhu, N. Wu, X. Zhao, Y. Wei, J. M. Zhou and Y. L. Song, *J. Mater. Chem. C*, 2019, **7**, 14069–14074.
37 Y. C. Li, L. Q. Chai, X. H. Wang, L. Zhou, Q. G. Fan and J. Z. Shao, *Materials*, 2018, **11**, 2500.
38 L. J. Cai, Y. Wang, L. Y. Sun, J. H. Guo and Y. J. Zhao, *Adv. Opt. Mater.*, 2021, **9**, 2100831.
39 L. W. Hao, J. D. Liu, Q. Li, R. K. Qing, Y. Y. He, J. Guo, G. Li, L. Zhu, C. Xu and C. Chen, *J. Mater. Sci. Technol.*, 2021, **81**, 203–211.
40 Y. Zhang, Y. Wang, Y. Wen, Q. Zhong and Y. J. Zhao, *ACS Appl. Mater. Interfaces*, 2020, **12**, 7486–7493.
41 L. Bai, Y. H. He, J. J. Zhou, Y. Lim, V. C. Mai, Y. H. Chen, S. Hou, Y. Zhao, J. Zhang and H. W. Duan, *Adv. Opt. Mater.*, 2019, **7**, 1900522.
42 P. Shen, Y. Zhang, Z. Cai, R. Liu, X. Xu, R. Li, J. J. Wang and D. A. Yang, *J. Mater. Chem. C*, 2021, **9**, 6944.

43 G. Y. Pan, J. Y. Yan, Z. L. Tang, J. H. Zhang, X. F. Lin, D. P. Yang, J. Y. Wu, W. J. Lin and G. B. Yi, *J. Mater. Chem. C*, 2022, **10**, 3959–3970.
44 G. Fu, X. Zhang, X. Chu, Y. Zhou and Y. L. Song, *Dyes Pigm.*, 2021, **95**, 109747.
45 Y. Li, Q. Fan, X. Wang, G. Liu, L. Chai, L. Zhou, J. Shao and Y. D. Yin, *Adv. Funct. Mater.*, 2021, **31**, 2010746.
46 M. Seong and D. G. Lee, *Curr. Microbiol.*, 2017, **74**, 661–670.
47 A. Ivask, A. ElBadawy, C. Kaweeteerawat, D. Boren, H. Fischer, Z. Ji, C. H. Chang, R. Liu, T. Tolaymat, D. Telesca, J. I. Zink, Y. Cohen, P. A. Holden and H. A. Godwin, *ACS Nano*, 2014, **8**, 374–386.
48 L. Bai, Y. Jin, X. Shang, H. Jin, Y. Zhou and L. Shi, *J. Mater. Chem. A*, 2021, **9**, 23916–23928.
49 L. Bai, Y. Jin, X. Shang, L. Shi, H. Jin, R. Zhou and S. Lai, *Chem. Eng. J.*, 2022, **438**, 135596.